J Neurophysiol 120: 2083–2090, 2018.
First published July 18, 2018; doi:10.1152/jn.00181.2018.

RESEARCH ARTICLE | *Higher Neural Functions and Behavior*

Chronic recording and electrochemical performance of Utah microelectrode arrays implanted in rat motor cortex

Bryan J. Black, Aswini Kanneganti, Alexandra Joshi-Imre, Rashed Rihani, Bitan Chakraborty, Justin Abbott, Joseph J. Pancrazio, and Stuart F. Cogan
Department of Bioengineering, The University of Texas at Dallas, Richardson, Texas

Submitted 14 March 2018; accepted in final form 16 July 2018

Black BJ, Kanneganti A, Joshi-Imre A, Rihani R, Chakraborty B, Abbott J, Pancrazio JJ, Cogan SF. Chronic recording and electrochemical performance of Utah microelectrode arrays implanted in rat motor cortex. *J Neurophysiol* 120: 2083–2090, 2018. First published July 18, 2018; doi:10.1152/jn.00181.2018.—Multisite implantable electrode arrays serve as a tool to understand cortical network connectivity and plasticity. Furthermore, they enable electrical stimulation to drive plasticity, study motor/sensory mapping, or provide network input for controlling brain-computer interfaces. Neurobehavioral rodent models are prevalent in studies of motor cortex injury and recovery as well as restoration of auditory/visual cues due to their relatively low cost and ease of training. Therefore, it is important to understand the chronic performance of relevant electrode arrays in rodent models. In this report, we evaluate the chronic recording and electrochemical performance of 16-channel Utah electrode arrays, the current state-of-the-art in pre-/clinical cortical recording and stimulation, in rat motor cortex over a period of 6 mo. The single-unit active electrode yield decreased from 52.8 ± 10.0 (*week 1*) to 13.4 ± 5.1% (*week 24*). Similarly, the total number of single units recorded on all electrodes across all arrays decreased from 106 to 15 over the same time period. Parallel measurements of electrochemical impedance spectra and cathodic charge storage capacity exhibited significant changes in electrochemical characteristics consistent with development of electrolyte leakage pathways over time. Additionally, measurements of maximum cathodal potential excursion indicated that only a relatively small fraction of electrodes (10–35% at 1 and 24 wk postimplantation) were capable of delivering relevant currents (20 μA at 4 nC/ph) without exceeding negative or positive electrochemical potential limits. In total, our findings suggest mainly abiotic failure modes, including mechanical wire breakage as well as degradation of conducting and insulating substrates.

NEW & NOTEWORTHY Multisite implantable electrode arrays serve as a tool to record cortical network activity and enable electrical stimulation to drive plasticity or provide network feedback. The use of rodent models in these fields is prevalent. We evaluated chronic recording and electrochemical performance of 16-channel Utah electrode arrays in rat motor cortex over a period of 6 mo. We primarily observed abiotic failure modes suggestive of mechanical wire breakage and/or degradation of insulation.

chronic recording; electrical stimulation; rodent models; Utah electrode array

INTRODUCTION

Implantable microelectrode arrays are being developed for chronic intracortical recording and stimulation applications, including control of brain-computer interfaces (Brandman et al. 2017; Jarosiewicz et al. 2015), restoration of lost sensory function (e.g., hearing, vision; Dobelle et al. 1979; Lowery et al. 2015; Schmidt et al. 1996), and motor/sensory mapping for studies of cortical plasticity (Abe et al. 2015). Although the clinical translation of these devices has been limited by consistent observations of reduced recording efficiency over time, due to a combination of both biotic and abiotic failure modes (Barrese et al. 2013; Jorfi et al. 2015), intracortical electrode arrays remain an important tool for basic neuroscience studies of functional brain mapping and plasticity. Even in this context, however, the general usefulness of a chronically implanted intracortical electrode array may be limited by its inability to *1*) consistently and chronically record extracellular action potentials with sufficient signal-to-noise ratios (SNR) and temporal resolution to discriminate single units or *2*) deliver suprathreshold electrical stimulation without exceeding the water electrolysis threshold for chronic applications (3–6 mo) (Gillani et al. 2010; Markus et al. 2005; Ramos-Cabrer et al. 2010; Shin et al. 2014).

Utah electrode arrays (UEAs; Blackrock Microsystems) are the current state-of-the-art device for multisite, high-density recording/stimulation applications in the brain (Karumbaiah et al. 2013). Rats are a frequently used model in studies of motor cortex injury and recovery (Fluri et al. 2015; Khodaparast et al. 2014) as well as restoration of auditory/visual cues (Engineer et al. 2014, 2017; Witten et al. 2014) because of their relatively low cost, ease of training, and the existence of well-established behavioral models (Crawley 2003; van der Staay et al. 2009). However, to date, only two previous studies have reported on chronic recording performance or applications of UEAs in rat cortex over even a 3-mo period (Cody et al. 2018; Nolta et al. 2015), and importantly, no previous study has fully characterized the chronic electrical performance of UEAs in rat cortex.

In this study, we report both the recording and electrical performance of Blackrock UEAs implanted in rat motor cortex over a 6-mo period. Single-unit recordings were collected from motor cortex of lightly anesthetized rats with the use of parylene-C-encapsulated silicon-based Utah microelectrode arrays with sputtered iridium oxide (SIROF) electrode coatings. Electrochemical measurements of charge storage capacity,

Address for reprint requests and other correspondence: S. F. Cogan, Dept. of Bioengineering, The University of Texas at Dallas, 800 W. Campbell Rd., Bioengineering and Sciences Building 13.601, Richardson, TX 75080 (e-mail: stuart.cogan@utdallas.edu).

electrochemical impedance spectra, and charge injection capacity were collected from lightly anesthetized rats over the same period of time. Our data indicate that the single-unit recording capability is significantly reduced 6 mo following implantation and that this reduction is attributable to a combination of mechanical device failure and the development of electrolyte leakage pathways.

MATERIALS AND METHODS

UEA implantation. All procedures were carried out in accordance with protocols approved by the Institutional Animal Care and Use Committee at the University of Texas at Dallas. Unilateral UEA implantation was carried out largely as previously described (Nolta et al. 2015). Briefly, adult male rats (330–380 g, aged 9–15 wk) were initially anesthetized by intraperitoneal injection of a ketamine (65 mg/kg)-xylazine (13.33 mg/kg)-acepromazine (1.5 mg/kg) cocktail (KXA). Following confirmation of surgical depth anesthesia, rats were positioned onto a stereotaxic frame with a hydraulic/electronic micropositioner (model 940; Kopf Instruments) that supplied a constant flow of 1.5% isoflurane mixed with 100% O_2. Blood pressure, heart rate, and rectal temperature were monitored throughout each surgery. Local anesthetic (lidocaine) was injected along the midline region of the skull before incision. A single primary incision was made along the midline, from the anterior frontal bone (between the eyes) to the posterior base of the parietal bone, exposing the temporalis muscles and periosteum. These were reflected and fixed into position using hemostatic clamps to expose the skull. A roughly 2-mm × 2-mm square craniotomy was created above the motor cortex region (right rostral, relative to the bregma). Three support screws were placed to support the head cap; two in the parietal bone (right and left) and one in the frontal bone, opposite the craniotomy site.

The dura mater was reflected and the SIROF-tipped, parylene-C-encapsulated array (1-mm shank length) was inserted to a depth of 1 mm using a high-speed pneumatic inserter (Blackrock Microsystems). Platinum ground and reference wires from the Omnetics connector were wrapped at least three times around the rostral and caudal (left) bone screws, respectively. A collagen-based dural graft (Biodesign dural graft; Cook Medical) was replaced on top of the array and exposed brain. A thin layer of silicone elastomer gel (Kwik-Cast; WPI) was then used to fill the craniotomy region. After the elastomer was allowed to set, the head cap was formed using dental bone cement, encapsulating the implantation region as well as the bone screws and ground/reference wires. Finally, the skin was closed around the percutaneous Omnetics connector using stainless steel Autoclip surgical staples (MikRon Precision). The rats were then transferred back to their enclosures on a heating pad and monitored for recovery.

Voltage transients. In vivo voltage transient measurements were recorded weekly from anesthetized animals using a PlexStim electrical stimulator system (Plexon). Animals were lightly anesthetized using 1.7% isoflurane to minimize artifacts and noise. The experiment was performed in a three-electrode system using a Ag-AgCl reference electrode and a platinum counter electrode attached to the proximal and distal end of the animal's tail, respectively. Measurements were made by applying biphasic, cathodal first, current pulses with a pulse

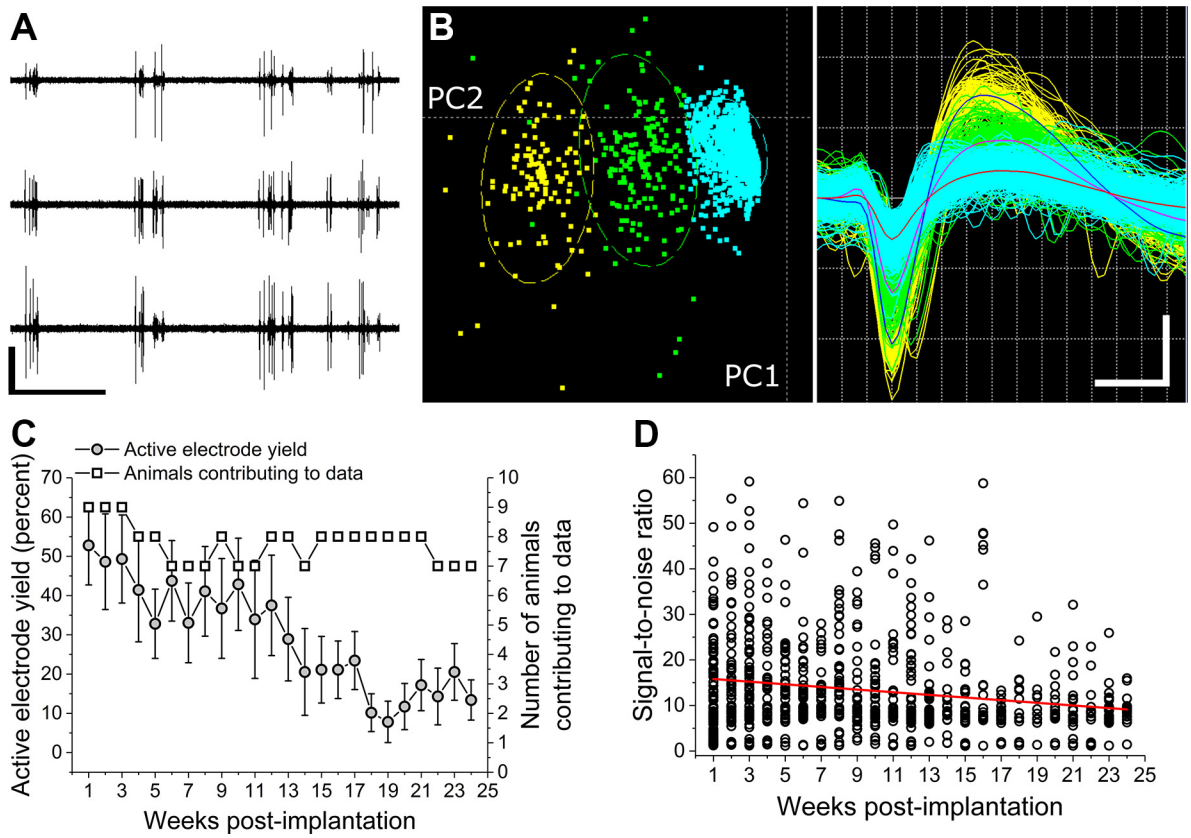

Fig. 1. Chronic single-unit recordings from rat motor cortex using parylene-C-encapsulated sputtered iridium oxide 16-channel Utah electrode arrays (UEAs). *A*: filtered continuous recordings from 3 electrodes on a single UEA (*week 1*) indicating simultaneous multisite, network activity. Vertical and horizontal scale bars represent 75 μV and 5 s, respectively. *B*: representative unit sorting based on amplitude and separation in 2-dimensional principle component space (PC1 and PC2; *left*) and resulting color-coded single units (*right*). The dashed ellipses represent the sorted unit's standard deviations along the principal axes. Vertical and horizontal scale bars represent 50 μV and 0.3 ms, respectively. *C*: percentage of electrode recording single units per array (*left y*-axis, active electrode yield) over 24 wk in vivo (means ± SE) as well as the number of animals contributing to each week's data (*right y*-axis). *D*: signal-to-noise ratio of the largest amplitude single unit on each electrode. Data represents all units across all electrodes across all arrays. Red line represents linear fitting of the data.

width of 200 μs, interphase delay of 100 μs, 50-Hz frequency, with an incrementing amplitude of 0.5 or 1 μA, up to 20 μA (4 nC/ph). The combined use of an oscilloscope and MATLAB code allowed for controlled stimulation that stopped incrementing current at either the desired maximum current or when the water reduction or oxidation potential for the iridium oxide electrodes (−0.6 to 0.8 V) was reached, whichever was reached first. The use of a biphasic pulse and this MATLAB program allowed for a charge-balanced pulse that was safe for the animal and did not result in excessive polarization of the microelectrode during stimulation. Voltage transient data was used to find the maximum cathodal potential excursion (E_{mc}), which was defined as the electrode potential measured 12 μs after the cathodal current pulse went to zero so that the voltage transient was no longer influenced by ohmic voltage drops in the surrounding tissue.

Single-unit recordings and processing. In vivo electrophysiological recordings were performed once per week, beginning 1 wk postimplantation. Animals were lightly anesthetized using 1.7% isoflurane, and UEAs were connected externally via an HST/16D Gen2 16-channel headstage to the Digital Headstage Processor (Plexon) for analog-to-digital conversion. Wide-band data (0.1–7,000 Hz) were collected from all 16 recording electrodes simultaneously at a 40,000-Hz sampling rate for 10 min using Plexon's Omniplex chassis and PlexControl software. For single-unit detection and discrimination, wide-band data were ban-pass filtered (250–7,000 Hz) using a four-pole Butterworth filter, and a threshold was set at 4σ based on root mean square (RMS) noise. Single units were manually sorted on the basis of amplitude and principal component space analysis. SNR was calculated as

$$SNR = \left(\frac{Signal}{RMS_{Noise}} \right),$$

where RMS_{Noise} was calculated from the entire filtered continuous recording. Additional processing and analysis was carried out using Plexon's Offline Sorter, NeuroExplorer (Nex Technologies) software, and a boutique MATLAB script.

Cyclic voltammetry and electrochemical impedance spectroscopy. Both in vitro and in vivo electrochemical measurements were carried out using a GAMRY Reference 600 potentiostat in a three-electrode configuration (working, counter, and reference). In vitro measurements were carried out in an inorganic model interstitial fluid (ISF) at 37°C (Cogan et al. 2007). In the case of in vivo measurements, reference and counter electrodes were secured to the animal's tail and wrapped with gauze soaked in phosphate-buffered saline to ensure electrical contact throughout the measurements.

Cyclic voltammograms (CVs) were recorded at sweep rates of 50 and 50,000 mV/s between potential limits of −0.6 and 0.8 V vs. Ag-AgCl. Three consecutive CV cycles were run, and the charge storage capacity of the SIROF electrode was determined on the third CV cycle from the time integral of the cathodal current using methods described previously (Cogan 2008). The electrochemical impedance spectroscopy (EIS) measurements were made around the SIROF open-circuit potential using a sinusoidal 10-mV RMS excitation. The impedance spectra were acquired over a frequency range of 1 to 10^5 Hz with a step size of 10 points per decade.

Statistical analysis. Statistical analysis and graphing were carried out using OriginPro 2017 (Origin Laboratory, Northampton, MA). In all cases, significance of increasing/decreasing trends was determined by ANOVA, with $P < 0.05$ considered significant. Subsequent calculations of Spearman's correlation coefficients (r_s) were carried out, with calculation of P values based on two-tailed tests and $P < 0.05$ considered significant. In the case of SNR comparisons between *weeks 1* and *24*, significance was determined by paired-sample *t*-test, with $P < 0.05$ considered significant. In the case of EIS measurements, a multitiered Grubb's test (maximum or 4 tiers) was applied at a 0.05 significance level to exclude outliers.

RESULTS

Single- and multiunit in vivo recordings. To evaluate the chronic recording performance of UEAs in a rat model, we implanted unilaterally the motor cortex of 10 Long Evans rats (330–380 g, aged 9–15 wk) with SIROF microelectrode arrays (1-mm shank length), which were tethered to external Omnetics connectors attached to the skull. In vivo electrophysiological recordings were performed each week for 6 mo beginning 1 wk postimplantation. Of the 10 implanted animals, 7 reached the 6-mo end point. Of the three that did not reach the terminal date, one suffered mechanical detachment of the head cap (28 days postimplantation) and two expired of unknown causes (154 and 162 days postimplantation). As a precaution, single animals were sometimes excluded from electrophysiological recording sessions or electrochemical measurements due to either minor head cap issues (i.e., apparent inflammation or bleeding) or, in the case of one animal, adverse reaction to inhaled anesthetic (isoflurane).

Figure 1*A* shows filtered continuous recordings from three representative electrodes on the same UEA, postimplantation *week 1*. At this time point, significant signal deflections (>4σ, based on RMS noise calculations) were detected across multiple electrodes on each implanted array with excellent SNR (14.2 ± 2.1, mean ± SE) and were found to correspond in time across electrodes, consistent with all-or-nothing action poten-

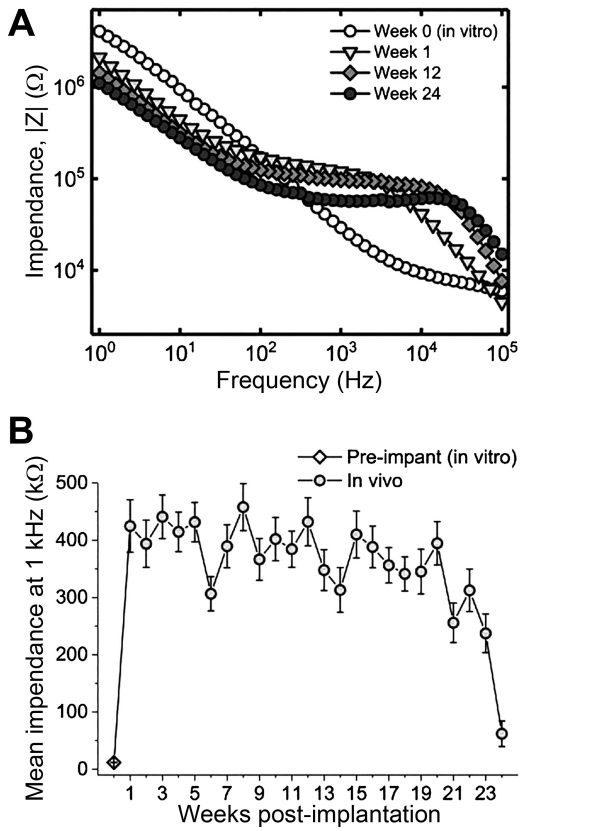

Fig. 2. Electrochemical impedance spectroscopy (EIS). *A*: representative traces of EIS spectrum for an electrode reporting single units through postimplantation *week 24*. Open circles (*week 0*) represent data from preimplantation in vitro recordings in model interstitial fluid (ISF). *Z*, impedance magnitude. *B*: mean (±SE) impedances for all electrodes across all arrays over 24 wk in vivo. Open diamond (*week 0*) represents preimplantation measurement in model ISF. Outlier impedance values, as identified by multitiered Grubb's test, were excluded from further analysis.

tials and network-level activity. These single action potentials could be further discriminated (sorted), based on characteristic time course and shape, into single units (Fig. 1*B*). One week following implantation, 52.8 ± 10.0% of electrodes per array exhibited at least one sorted unit (termed "active electrode yield"), with the total number of sorted units across all arrays equaling 106. By postimplantation *week 24*, the active electrode yield was reduced to 13.4 ± 5.1% and the total number of sortable units was reduced to 15 (Fig. 1*D*). In both cases, linear fitting of the data confirmed decreasing trends (negative slopes) that were significantly different from zero ($P < 0.001$, ANOVA). Additionally, we observed a significant reduction in mean SNR between *weeks 1* (14.2 ± 2.1) *and 24* (8.9 ± 0.8), based on a paired-sample *t*-test (Fig. 1*E*), and, again, linear fitting of the data confirmed a significant decreasing trend ($P < 0.001$, ANOVA). Because our threshold for single units was based on the standard deviation of RMS noise, we also calculated the percentage coefficient of variation (%CV) across all arrays for all time points. Following postimplantation *week 3*, the %CV was consistently between 12% and 32% and did not exhibit a significant trend in either the positive or negative direction (data not shown).

Electrochemical impedance spectroscopy and cyclic voltammetry. To better elucidate possible time-dependent failure modes in vivo, we performed EIS and CV measurements in parallel with the electrophysiological recordings. EIS and CV measurements were carried out on lightly anesthetized rats to minimize motion artifacts, as previously reported (Kane et al. 2013; Ward et al. 2009). These measurements were carried out at least 24 h before or after electrophysiological recordings to limit the single-session isoflurane exposure to less than 2 h. Figure 2*A* shows the mean 1-kHz impedance magnitude before implantation (in vitro, carried out in model ISF) and in vivo on postimplantation *weeks 1*, *12*, and *24*. One week postimplantation, all electrodes exhibited a significant increase in 1-kHz impedance magnitude (424.7 ± 45.6 kΩ) vs. in vitro measurements (11.8 ± 0.5 kΩ). This level of multifold increase following implantation is highly consistent with previous observations of in vitro vs. in vivo impedances (Cogan 2008; Mercanzini et al. 2009; Musa et al. 2009; Prasad et al. 2012; Wang et al. 2013) and is attributable to tissue impedance and additional impedance at the electrode-electrolyte interface. Once implanted, the impedance value at 1 kHz remained largely consistent through *week 20* and then rapidly declined through *week 24* (62.0 ± 22.3 kΩ). Linear fitting of the 1-kHz impedance data (*weeks 20–24*) confirmed a significant reduction over that time period (Fig. 2*B*; $P < 0.001$, ANOVA). Furthermore, the mean 1-kHz impedance magnitude was found to positively correlate with both the mean active electrode yield ($r_s = 0.60$, $P = 0.002$, two-tailed test) and the total number of units recorded ($r_s = 0.68$, $P < 0.001$, two-tailed test). Because the observed reduction in impedance began well past time points typically associated with the onset of astrogliosis or fibrotic encapsulation (2–16 weeks; Karumbaiah et al. 2013; Nolta et al. 2015; Winslow et al. 2010), these data suggest that the impedance decreases between *weeks 20* and *24* may be abiotic and associated with an increase in accessible conductive surface area (e.g., delamination of the insulating material).

Cathodic charge storage capacity (CSC) was calculated from CV data at sweep rates of 50 and 50,000 mV/s. Higher sweep rates access conductive paths nearer the electrode tip, whereas lower sweep rates allow access to greater conductive surface area, proximal to the electrode tip. Figure 3, *A* and *C*, shows representative CV traces for sweep rates of 50 and 50,000 mV/s at in vitro and in vivo time points. One week postimplantation, we observed a slight decrease in the mean CSC at 50 mV/s (36 ± 3.1 mC/cm^2) and a significant decrease in CSC at 50,000 mV/s (1.3 ± 0.1 mC/cm^2) compared with that in vitro (55.5 ± 6.4 and 3.7 ± 0.3 mC/cm^2, respectively). In both cases, the CSCs increased over the indwelling period, reaching

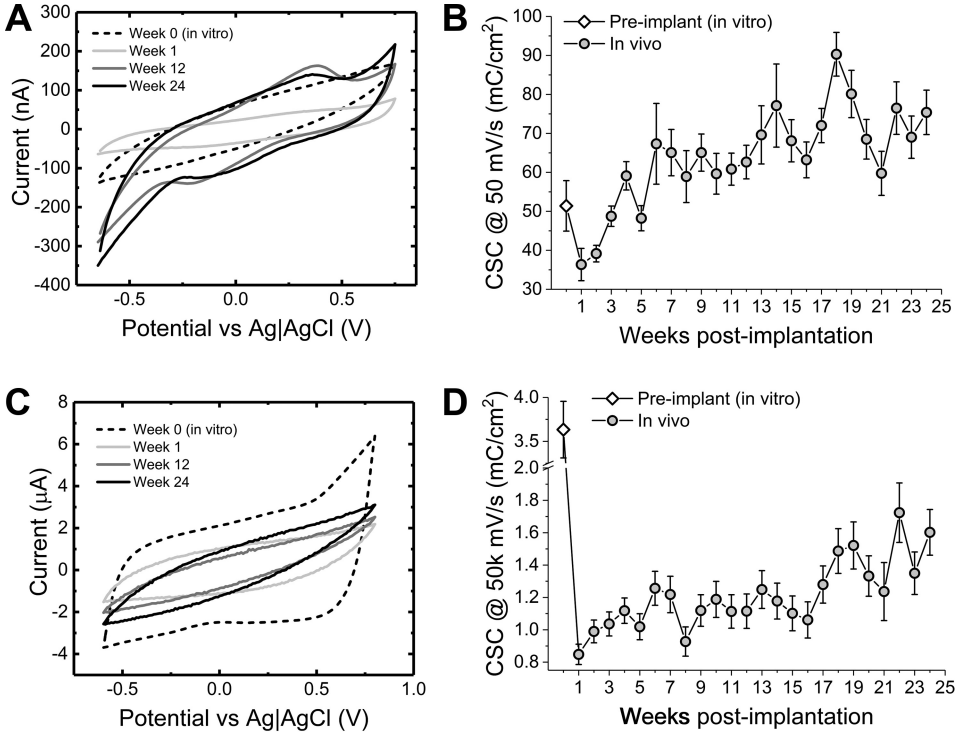

Fig. 3. Charge storage capacity (CSC) measurements via cyclic voltammetry (CV) at 50 and 50,000 mV/s sweep rates. *A*: representative CV trace (sweep rate of 50 mV/s) for a single electrode at postimplantation *weeks 1*, *12*, and *24*. Dashed line (*week 0*) represents preimplantation in vitro measurements in model interstitial fluid (ISF). *B*: mean (±SE) CSC for all electrodes across all arrays for 24 wk in vivo. Open diamond (*week 0*) represents preimplantation in vitro values in model ISF. *C*: representative CV trace (sweep rate of 50,000 mV/s) for a single electrode at postimplantation *weeks 1*, *12*, and *24*. Dashed line (*week 0*) represents preimplantation in vitro measurements in model ISF. *D*: mean (±SE) CSC for all electrodes across all arrays for 24 wk in vivo. Open diamond (*week 0*) represents preimplantation in vitro values in model ISF. Ag-AgCl, reference electrode.

74.2 ± 5.6 and 1.8 ± 0.1 mC/cm^2 by postimplantation *week 24* (Fig. 3, *B* and *D*). Linear fitting of the data confirmed significantly increasing trends ($P < 0.001$, two-tailed test). Furthermore, the mean CSCs at both 50 and 50,000 mV/s were found to have strong negative correlations with both the mean active electrode yield ($r_s = -0.78, -0.77$) and total number of units recorded ($r_s = -0.84, -0.84$). In each case, the correlations were highly significant ($P < 0.001$, two-tailed test). These findings further suggest loss of units over time may be associated with the development of current leakage pathways, because increasing CSC (especially at lower sweep rates) implies increased access to conductive surface area. This access may be due to the formation of pinholes or cracks, or may be due to separation of the insulating from conductive materials.

Voltage transient measurements. To evaluate whether Blackrock Microsystem UEAs may be used for chronic stimulation applications in rats, we measured the percentage of electrodes capable of delivering a minimum charge injection of 4 nC/ph without exceeding the maximum negative or positive electrochemical potential limits (E_{mc}, E_{ma}) associated with water reduction ($E_{mc} = -0.6$ V vs. Ag-AgCl) or oxidation ($E_{ma} = 0.8$ V vs. Ag-AgCl) (Fig. 4*A*). Voltage transient measurements were carried out immediately following electrophysiological recordings while animals were still lightly anesthetized. Surprisingly, only 10% of electrodes were capable of delivering 4 nC/ph (20-μA, 200-μs pulses) 1 week postimplantation without reaching or exceeding either the water reduction or oxidation threshold. Although we observed an increasing trend during the indwelling period, this percentage never exceeded 35.7% (*week 22*) and only reached 34.3% on postimplantation *week 24* (Fig. 4*B*). Several stimulation applications associated with motor tasks (Seong et al. 2014; Wang et al. 2013) report a threshold of 75–100 μA. These data suggest that Blackrock Microsystem UEAs may have limitations with respect to chronic stimulation applications in the rat cortex. Furthermore, because charge injection capacity is dependent on electrode surface area, the increasing percentage of "passing" electrodes suggests access to greater electrode conductive surface area. Linear fitting of the data confirmed a significantly increasing trend in passing electrodes ($P < 0.001$, ANOVA) with time. Additionally, these data were found to have a strong negative correlation with both the mean active electrode yield ($r_s = -0.87$, $P < 0.001$, two-tailed test) and the total number of units ($r_s = -0.88$, $P < 0.001$, two-tailed test). In total, the data are consistent with an increasing electrolyte accessibility to conductive surfaces under insulation over time, due, at least in part, to compromised integrity of the parylene-C or its reduced adhesion to the silicon superstructure of the array.

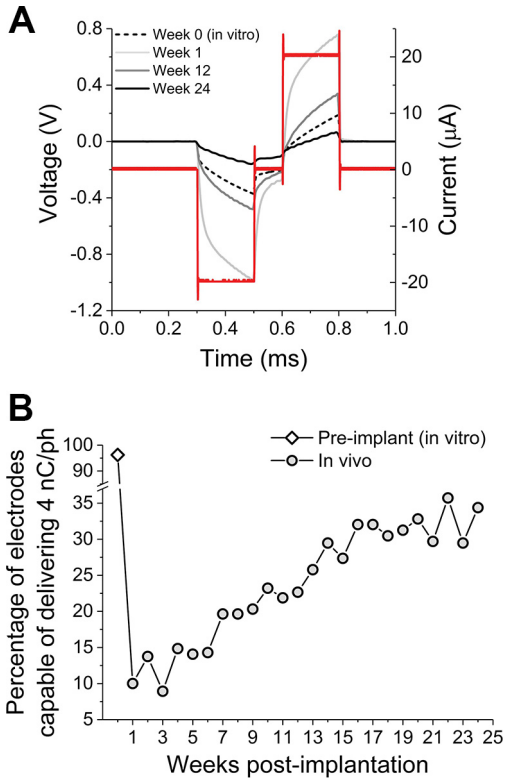

Fig. 4. Evaluation of charge injection capacity based on ability to deliver 4 nC/ph within the ±threshold for water electrolysis. *A*: representative voltage traces (left *y*-axis, grayscale) during pulsed current injection (red trace, *right y*-axis) from a single electrode at postimplantation *weeks 1*, *12*, and *24*. Dashed line (*week 0*) represents preimplantation in vitro measurement in model interstitial fluid (ISF). *Week 1* voltage trace represents a failed trial; maximum cathodal potential excursion (E_{mc}) exceeds −0.6 V. *Weeks 0*, *12*, and *24* were considered passing conditions (successful delivery of 4 nC/ph without E_{mc} less than −0.6 V). Constant pulse parameters are cathodic leading, biphasic, 200-μs phase width, 100-μs interphase duration. *B*: percentage of electrodes capable of delivering 4 nC/ph over 24 wk in vivo. These percentages represent calculation across all electrodes across all arrays. Open diamond (*week 0*) represents in vitro preimplantation measurement in model ISF.

Immunohistochemistry and explant failure analysis. It is well established that the loss of recording or stimulation function with implantable electrode arrays depends on multiple factors (Barrese et al. 2016). Previous studies in cats, nonhuman primates, rats, and even humans have established modes of failure that may be conserved across array type and species and that are mechanical, electrical, or immunological in nature (Barrese et al. 2013; Cody et al. 2018; Jorfi et al. 2015; Karumbaiah et al. 2013; Sillay et al. 2013). In this study, we have observed indications of all three, although our loss of units may be attributed primarily to mechanical and electrical failure modes. Of the 10 implanted arrays, only 4 exhibited single units by *week 24*. In the case of three arrays, loss of units could be directly attributed to either mechanical failure of the head cap ($n = 1$) or breakage of the wire bundle ($n = 2$). Three additional arrays, after explanation, exhibited EIS profiles in saline that were consistent with disconnected wires (Fig. 5), although no apparent breakage along the bundle or detachment at the bonding pads was observed. Of those not exhibiting modes of mechanical device failure, we observed significant reduction in both the total number of units recorded as well as the associated SNRs over time. As previously mentioned, our findings from parallel in vivo EIS and CV measurements suggest increased access to conductive surface area (degradation of insulating material), resulting in decreased impedance at 1 kHz, increased charge storage capacity, and reduced SNR associated with a decrease in single-unit amplitudes.

To evaluate the contribution of the foreign body response to reduced recording performance, brain tissue was sliced and stained to identify astrocytes, activated microglia, and neurons. Before histological analysis, we observed fibrotic encapsulation (Fig. 6, *A* and *B*) consistent with previous findings in both rat (Cody et al. 2018) and monkey (Barrese et al. 2013). However, we did not find any direct correspondence between

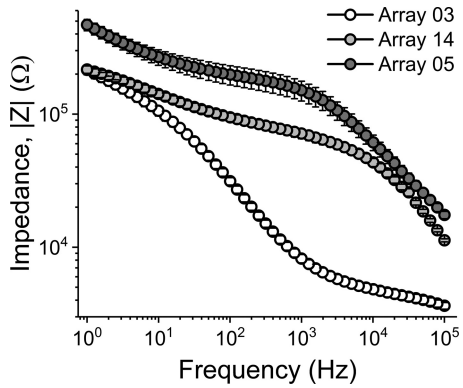

Fig. 5. Representative electrochemical impedance spectroscopy (EIS) traces for 3 explanted arrays that exhibited units throughout the indwelling period (*array 03*), sudden drop-off in units corresponding with apparent wire breakage (*array 14*), and sudden drop-off in units with no observable wire breakage but an EIS that suggests disconnected electrodes (*array 05*). *Z*, impedance magnitude.

the presence of this residual encapsulation on an explanted array and the ability of that array to record single units. Figure 6, *C* and *D*, shows representative immunohistochemistry outcomes at depths of ~200–400 μm and 1.2 mm. We observed substantial tissue loss near the center base of the array, which may be due to either adhesion to the explanted array or tissue loss during the indwelling period. This is highly consistent with histological outcomes reported in Nolta et al. (2015) for both chronically indwelling arrays and stab-type injuries. However, the loss of tissue between individual shanks made it impossible to investigate direct correlations between encapsulation and recording performance of individual electrodes.

DISCUSSION

In this article, we report the chronic recording and electrochemical performance of parylene-C-encapsulated UEAs implanted in rat motor cortex. The recording performance of these arrays was found to significantly decrease over the 24-wk (6 mo) indwelling period in terms of both active electrode yield and SNR. Conversely, charge injection capacities were found to increase over time. However, initial charge injection capacity was poor, with only 10% of electrodes able to deliver 4 nC/ph on postimplantation *week 1*. This threshold is significantly lower than those previously described as sufficient to characterize stimulus efficacy for evoking motor movements (Wang et al. 2013) or to generate stimulation-based maps of the motor cortex (Seong et al. 2014) in rat. Moreover, the increase in charge injection capacity over time suggests increased access to conductive surface area, further indicating electrical failure of the devices.

Although we observed significant reduction in active electrode yield over time, the present findings represent a signifi-

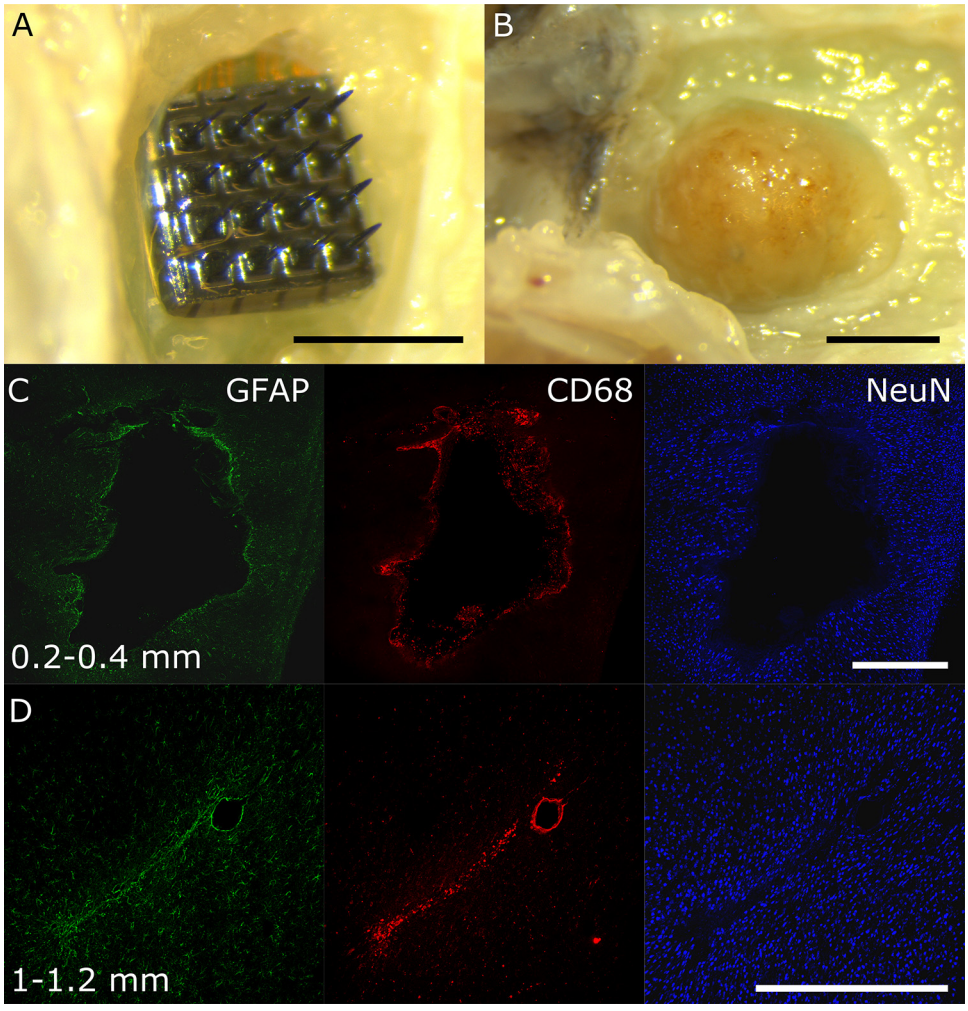

Fig. 6. Gross histological outcomes and failure analysis following device explantation. *A* and *B*: representative images of 2 gross fibrotic encapsulation outcomes, no observable encapsulation (*A*) and fully encapsulated (*B*). Scale bar, 1 mm. *C* and *D*: representative immunohistochemistry outcomes at a depth of 200–400 μm relative to the Utah electrode array base. *C* and *D*: individual fluorescence channel images associated with 3 histological markers for astrocytes: glial fibrillary acidic protein (GFAP; green), activated microglia/macrophages (CD68; red), and neuronal nuclei (NeuN; blue), at depths of ~0.2–0.4 (*C*) and 1–1.2 mm (*D*) from the surface of the brain. Scale bars, 1 mm.

cant improvement compared with previous studies using Utah arrays in rat (Cody et al. 2018; Nolta et al. 2015). We believe that this may be attributable to three differences in animal handling or surgical methodologies identified in either one or both of these studies. *1*) In the present study, all animals were fitted with Elizabethan collars immediately following implantation to help prevent manipulation of the implantation site. *2*) We used a pneumatic inserter for ballistic implantation (speeds ≥1 m/s). Previous studies in rat have used micromanipulators to implant at speeds of ~1 mm/min (Cody et al. 2018), or the arrays were manually pushed in with handheld forceps (Nolta et al. 2015). Although the question of optimal insertion speed (fast, slow, or ballistic) depends on many factors and continues to be a point of debate (Polikov et al. 2005), there is at least one school of thought that supports high-speed insertion due to observations of decreased tearing (Edell et al. 1992) or dimpling (Hosseini et al. 2007) of the tissue. *3*) We also included a layer of dural graft between the back side of the electrode array and the elastomer gel (Kwik-Sil), which served as a structural support between the array and head cap. Surgeries in larger mammalian species have classically closed and sutured the dura over the back side of the array (Sharma et al. 2015). However, that is problematic in smaller species, where the array-to-brain size ratio is much larger. Previous studies in rat have reported the use of elastomer gel only (Cody et al. 2018) or have not reported any steps taken to reseal the disrupted dura mater (Kim et al. 2004; Nolta et al. 2015). The introduction of a dural graft may provide an alternative substrate for activated fibroblasts to prevent invasion onto the array and increase the rate of healing, reducing blood-brain barrier disruption and cerebrospinal fluid leakage over time.

It is worth mentioning that, though the time to failure may have been extended, the mechanical failure modes reported in this study are similar to those previously reported (mechanical wire breakage, development of leakage pathways). However, although we did observe glial and fibrotic encapsulation of the electrode arrays, we did not find any general correspondence between the histological outcomes and the ability to resolve single units. Moreover, the time to failure remained significantly shorter than that reported in studies of larger mammalian species, including nonhuman primates. Previous studies have suggested that this may be attributable to stresses incurred by ever-increasing animal skull thickness, which continues over the adolescent and adult lifetime of rats, especially males (Nolta et al. 2015; Nolta 2016).

In summary, our measurements of single-unit recording performance in combination with in vivo electrochemical characterization suggest that these UEAs may have limited utility for chronic studies of cortical plasticity changes or motor evoked responses in rat, which require stable recording and/or stimulation capabilities for 3–6 mo.

GRANTS

This research was funded by Department of Defense Advanced Research Projects Agency Grant HR0011-15-2-0017 (to J. J. Pancrazio and S. F. Cogan).

DISCLOSURES

No conflicts of interest, financial or otherwise, are declared by the authors.

AUTHOR CONTRIBUTIONS

J.J.P. and S.F.C. conceived and designed research; B.J.B., A.K., R.R., B.C., and J.A. performed experiments; B.J.B., A.K., R.R., B.C., and J.A. analyzed data; B.J.B., A.J.-I., J.J.P., and S.F.C. interpreted results of experiments; B.J.B. prepared figures; B.J.B. drafted manuscript; B.J.B., A.K., A.J.-I., J.J.P., and S.F.C. edited and revised manuscript; B.J.B., A.K., A.J.-I., R.R., B.C., J.A., J.J.P., and S.F.C. approved final version of manuscript.

REFERENCES

Abe H, McManus JN, Ramalingam N, Li W, Marik SA, Borgloh SM, Gilbert CD. Adult cortical plasticity studied with chronically implanted electrode arrays. *J Neurosci* 35: 2778–2790, 2015. doi:10.1523/JNEUROSCI.3579-14.2015.

Barrese JC, Aceros J, Donoghue JP. Scanning electron microscopy of chronically implanted intracortical microelectrode arrays in non-human primates. *J Neural Eng* 13: 026003, 2016. doi:10.1088/1741-2560/13/2/026003.

Barrese JC, Rao N, Paroo K, Triebwasser C, Vargas-Irwin C, Franquemont L, Donoghue JP. Failure mode analysis of silicon-based intracortical microelectrode arrays in non-human primates. *J Neural Eng* 10: 066014, 2013. 10.1088/1741-2560/10/6/066014.

Brandman DM, Cash SS, Hochberg LR. Review: Human intracortical recording and neural decoding for brain-computer interfaces. *IEEE Trans Neural Syst Rehabil Eng* 25: 1687–1696, 2017. doi:10.1109/TNSRE.2017.2677443.

Cody PA, Eles JR, Lagenaur CF, Kozai TD, Cui XT. Unique electrophysiological and impedance signatures between encapsulation types: an analysis of biological Utah array failure and benefit of a biomimetic coating in a rat model. *Biomaterials* 161: 117–128, 2018. doi:10.1016/j.biomaterials.2018.01.025.

Cogan SF. Neural stimulation and recording electrodes. *Annu Rev Biomed Eng* 10: 275–309, 2008. doi:10.1146/annurev.bioeng.10.061807.160518.

Cogan SF, Troyk PR, Ehrlich J, Gasbarro CM, Plante TD. The influence of electrolyte composition on the in vitro charge-injection limits of activated iridium oxide (AIROF) stimulation electrodes. *J Neural Eng* 4: 79–86, 2007. doi:10.1088/1741-2560/4/2/008.

Crawley JN. Behavioral phenotyping of rodents. *Comp Med* 53: 140–146, 2003.

Dobelle WH, Quest DO, Antunes JL, Roberts TS, Girvin JP. Artificial vision for the blind by electrical stimulation of the visual cortex. *Neurosurgery* 5: 521–527, 1979. doi:10.1227/00006123-197910000-00022.

Edell DJ, Toi VV, McNeil VM, Clark LD. Factors influencing the biocompatibility of insertable silicon microshafts in cerebral cortex. *IEEE Trans Biomed Eng* 39: 635–643, 1992. doi:10.1109/10.141202.

Engineer CT, Centanni TM, Im KW, Kilgard MP. Speech sound discrimination training improves auditory cortex responses in a rat model of autism. *Front Syst Neurosci* 8: 137, 2014. doi:10.3389/fnsys.2014.00137.

Engineer CT, Shetake JA, Engineer ND, Vrana WA, Wolf JT, Kilgard MP. Temporal plasticity in auditory cortex improves neural discrimination of speech sounds. *Brain Stimul* 10: 543–552, 2017. doi:10.1016/j.brs.2017.01.007.

Fluri F, Schuhmann MK, Kleinschnitz C. Animal models of ischemic stroke and their application in clinical research. *Drug Des Devel Ther* 9: 3445–3454, 2015.

Gillani RL, Tsai SY, Wallace DG, O'Brien TE, Arhebamen E, Tole M, Schwab ME, Kartje GL. Cognitive recovery in the aged rat after stroke and anti-Nogo-A immunotherapy. *Behav Brain Res* 208: 415–424, 2010. doi:10.1016/j.bbr.2009.12.015.

Hosseini NH, Hoffmann R, Kisban S, Stieglitz T, Paul O, Ruther P. Comparative study on the insertion behavior of cerebral microprobes. *Conf Proc IEEE Eng Med Biol Soc* 2007: 4711–4714, 2007. doi:10.1109/IEMBS.2007.4353391.

Jarosiewicz B, Sarma AA, Bacher D, Masse NY, Simeral JD, Sorice B, Oakley EM, Blabe C, Pandarinath C, Gilja V, Cash SS, Eskandar EN, Friehs G, Henderson JM, Shenoy KV, Donoghue JP, Hochberg LR. Virtual typing by people with tetraplegia using a self-calibrating intracortical brain-computer interface. *Sci Transl Med* 7: 313ra179, 2015. doi:10.1126/scitranslmed.aac7328.

Jorfi M, Skousen JL, Weder C, Capadona JR. Progress towards biocompatible intracortical microelectrodes for neural interfacing applications. *J Neural Eng* 12: 011001, 2015. doi:10.1088/1741-2560/12/1/011001.

Kane SR, Cogan SF, Ehrlich J, Plante TD, McCreery DB, Troyk PR. Electrical performance of penetrating microelectrodes chronically implanted

in cat cortex. *IEEE Trans Biomed Eng* 60: 2153–2160, 2013. doi:10.1109/TBME.2013.2248152.

Karumbaiah L, Saxena T, Carlson D, Patil K, Patkar R, Gaupp EA, Betancur M, Stanley GB, Carin L, Bellamkonda RV. Relationship between intracortical electrode design and chronic recording function. *Biomaterials* 34: 8061–8074, 2013. doi:10.1016/j.biomaterials.2013.07.016.

Khodaparast N, Hays SA, Sloan AM, Fayyaz T, Hulsey DR, Rennaker RL 2nd, Kilgard MP. Vagus nerve stimulation delivered during motor rehabilitation improves recovery in a rat model of stroke. *Neurorehabil Neural Repair* 28: 698–706, 2014. doi:10.1177/1545968314521006.

Kim YT, Hitchcock RW, Bridge MJ, Tresco PA. Chronic response of adult rat brain tissue to implants anchored to the skull. *Biomaterials* 25: 2229–2237, 2004. doi:10.1016/j.biomaterials.2003.09.010.

Lowery AJ, Rosenfeld JV, Lewis PM, Browne D, Mohan A, Brunton E, Yan E, Maller J, Mann C, Rajan R, Rosa M, Pritchard J. Restoration of vision using wireless cortical implants: The Monash Vision Group project. *Conf Proc IEEE Eng Med Biol Soc* 2015: 1041–1044, 2015.

Markus TM, Tsai SY, Bollnow MR, Farrer RG, O'Brien TE, Kindler-Baumann DR, Rausch M, Rudin M, Wiessner C, Mir AK, Schwab ME, Kartje GL. Recovery and brain reorganization after stroke in adult and aged rats. *Ann Neurol* 58: 950–953, 2005. doi:10.1002/ana.20676.

Mercanzini A, Colin P, Bensadoun JC, Bertsch A, Renaud P. In vivo electrical impedance spectroscopy of tissue reaction to microelectrode arrays. *IEEE Trans Biomed Eng* 56: 1909–1918, 2009. doi:10.1109/TBME.2009.2018457.

Musa S, Welkenhuysen M, Prodanov D, Eberle W, Bartic C, Nuttin B, Borghs G. In vitro and in vivo electrochemical characterization of a microfabricated neural probe. *Conf Proc IEEE Eng Med Biol Soc* 2009: 7143–7146, 2009. doi:10.1109/IEMBS.2009.5335362.

Nolta NF. *Studies of intracortical microelectrode array performance and foreign body response in young and aged rats* (PhD dissertation). Salt Lake City, UT: University of Utah, 2016.

Nolta NF, Christensen MB, Crane PD, Skousen JL, Tresco PA. BBB leakage, astrogliosis, and tissue loss correlate with silicon microelectrode array recording performance. *Biomaterials* 53: 753–762, 2015. doi:10.1016/j.biomaterials.2015.02.081.

Polikov VS, Tresco PA, Reichert WM. Response of brain tissue to chronically implanted neural electrodes. *J Neurosci Methods* 148: 1–18, 2005. doi:10.1016/j.jneumeth.2005.08.015.

Prasad A, Xue QS, Sankar V, Nishida T, Shaw G, Streit WJ, Sanchez JC. Comprehensive characterization and failure modes of tungsten microwire arrays in chronic neural implants. *J Neural Eng* 9: 056015, 2012. doi:10.1088/1741-2560/9/5/056015.

Ramos-Cabrer P, Justicia C, Wiedermann D, Hoehn M. Stem cell mediation of functional recovery after stroke in the rat. *PLoS One* 5: e12779, 2010. doi:10.1371/journal.pone.0012779.

Schmidt EM, Bak MJ, Hambrecht FT, Kufta CV, O'Rourke DK, Vallabhanath P. Feasibility of a visual prosthesis for the blind based on intracortical microstimulation of the visual cortex. *Brain* 119: 507–522, 1996. doi:10.1093/brain/119.2.507.

Seong HY, Cho JY, Choi BS, Min JK, Kim YH, Roh SW, Kim JH, Jeon SR. Analysis on bilateral hindlimb mapping in motor cortex of the rat by an intracortical microstimulation method. *J Korean Med Sci* 29: 587–592, 2014. doi:10.3346/jkms.2014.29.4.587.

Sharma G, Annetta N, Friedenberg D, Blanco T, Vasconcelos D, Shaikhouni A, Rezai AR, Bouton C. Time stability and coherence analysis of multiunit, single-unit and local field potential neuron signals in chronically implanted brain electrodes. *Bioelectron Med* 2: 63–71, 2015.

Shin SS, Dixon CE, Okonkwo DO, Richardson RM. Neurostimulation for traumatic brain injury. *J Neurosurg* 121: 1219–1231, 2014. doi:10.3171/2014.7.JNS131826.

Sillay KA, Rutecki P, Cicora K, Worrell G, Drazkowski J, Shih JJ, Sharan AD, Morrell MJ, Williams J, Wingeier B. Long-term measurement of impedance in chronically implanted depth and subdural electrodes during responsive neurostimulation in humans. *Brain Stimul* 6: 718–726, 2013. doi:10.1016/j.brs.2013.02.001.

van der Staay FJ, Arndt SS, Nordquist RE. Evaluation of animal models of neurobehavioral disorders. *Behav Brain Funct* 5: 11, 2009. doi:10.1186/1744-9081-5-11.

Wang C, Brunton E, Haghgooie S, Cassells K, Lowery A, Rajan R. Characteristics of electrode impedance and stimulation efficacy of a chronic cortical implant using novel annulus electrodes in rat motor cortex. *J Neural Eng* 10: 046010, 2013. doi:10.1088/1741-2560/10/4/046010.

Ward MP, Rajdev P, Ellison C, Irazoqui PP. Toward a comparison of microelectrodes for acute and chronic recordings. *Brain Res* 1282: 183–200, 2009. doi:10.1016/j.brainres.2009.05.052.

Winslow BD, Christensen MB, Yang WK, Solzbacher F, Tresco PA. A comparison of the tissue response to chronically implanted Parylene-C-coated and uncoated planar silicon microelectrode arrays in rat cortex. *Biomaterials* 31: 9163–9172, 2010. doi:10.1016/j.biomaterials.2010.05.050.

Witten L, Oranje B, Mørk A, Steiniger-Brach B, Glenthøj BY, Bastlund JF. Auditory sensory processing deficits in sensory gating and mismatch negativity-like responses in the social isolation rat model of schizophrenia. *Behav Brain Res* 266: 85–93, 2014. doi:10.1016/j.bbr.2014.02.048.